

# A new index for mapping lichen-dominated biological soil crusts in desert areas

Jin Chen<sup>a,\*</sup>, Ming Yuan Zhang<sup>b</sup>, Le Wang<sup>c</sup>, Hiroto Shimazaki<sup>a</sup>, Masayuki Tamura<sup>a</sup>

<sup>a</sup>Key Laboratory of Environmental Change and Natural Disaster, Beijing Normal University, China

<sup>b</sup>Xinjiang Institute of Ecology and Geography, Chinese Academy of Sciences, China

<sup>c</sup>Texas Center for Geographic Information Science, United States

Received 13 September 2003; received in revised form 13 February 2005; accepted 19 February 2005

## Abstract

Tracking the presence, distribution and disappearance of biological soil crusts is important for ecosystem management of desert regions and provides highly valuable information on desertification and climate change studies in arid environments. Based on the analysis of the spectral features of biological soil crusts, we propose a new biological soil crust index (BSCI) for biological soil crusts mapping. Using both a radiative transfer simulation and an analysis of a Landsat Enhanced Thematic Mapper Plus (ETM+) image, we examined the ability of satellite remote sensing to detect and map biological soil crusts. Our simulation indicated that Landsat ETM+ data could be used, after atmospheric correction, to detect biological soil crusts if 33% or more of any pixel was accounted for by biological soil crusts. When the proposed BSCI was applied to the detection of biological soil crusts in the Gurbantonggut Desert, Xingjiang, China, a Kappa coefficient of 0.82 and an overall accuracy of 94.7% were achieved. These experimental results indicate that the new index is applicable to identification of lichen-dominated biological soil crusts, and therefore has good potential for biological soil crust detection and mapping in cool and cold deserts.

© 2005 Elsevier Inc. All rights reserved.

*Keywords:* Lichen; Biological soil crust; Desert

## 1. Introduction

Biological soil crusts<sup>1</sup> are communities of mosses, lichens, liverworts, algae, fungi, cyanobacteria and bacteria. Owing to their extraordinary abilities to survive desiccation and extreme temperatures (up to 70 °C), high pH and high salinity, biological soil crusts have been found in desert areas all over the world (Friedmann &

Galun, 1974; West, 1990). Notwithstanding their unassuming appearances, biological soil crusts play a significant role to assure the regular functioning of desert ecosystem, such as involvement in the process of formation, stability and fertility of soil, prevention of soil erosion caused by water or wind, augment of vascular plant colonization, and stabilization of sand dunes. A detailed discussion about ecological importance of biological soil crusts can be found in Belnap (2003), Belnap et al. (2001) and Eldridge and Greene (1994). On the other hand, biological soil crusts are extremely vulnerable to a variety of disturbances, such as climate change, intensified human activity, invasion by exotic annual grasses, and the successively increased fire risk. In addition, several field studies have reported that biological soil crusts possess a slow recovery rate, usually ranged from years to decades (Belnap & Eldridge, 2001; Brotherson et al, 1983; Johansen, 1993;

\* Corresponding author. Key Laboratory of Environmental Change and Natural Disaster, College of Resources Science and Technology, Beijing Normal University, Ministry of Education of China, Beijing 100875, China. Tel.: +86 10 58808149; fax: +86 10 58808178.

E-mail address: [chenjin@ires.cn](mailto:chenjin@ires.cn) (J. Chen).

<sup>1</sup> In the literature, biological soil crusts are also called cryptogamic, crytobiotic, microphytic, microfloral, organogenic, biogenic, and micro-biotic soil crusts.

Johansen et al., 1993). Given the aforementioned considerations, biological soil crusts have been recommended as the top management priority in desert regions (Belnap, 2003), especially under recent conditions in which desert regions are experiencing global warming and increasing human activity. As preliminary work to protect biological soil crusts in desert regions, it is important and necessary to identify the distribution of biological soil crusts and monitor their spatial and temporal changes. Such information is also invaluable for desertification and climate change studies. Remote sensing techniques have provide a great prospect to detect and map the spatial distribution

of biological soil crusts on a regional scale with a timely and efficient fashion (Karnieli et al., 2001).

In the past two decades, as a result of the increasing recognition of the ecological importance of biological soil crusts in desert regions, a number of research studies have been conducted to investigate the spectral characteristics of biological soil crusts or its species components (Ager & Milton, 1987; Graetz & Gentle, 1982; Jacobberger, 1989; Karnieli & Sarafis, 1996; Karnieli & Tsoar, 1995; Karnieli et al., 1999; Karnieli et al., 1997; Karnieli et al., 1996; O’Neill, 1994; Pinker & Karnieli, 1995; Rollin et al., 1994; Tsoar & Karnieli, 1996). Other works in this field mainly

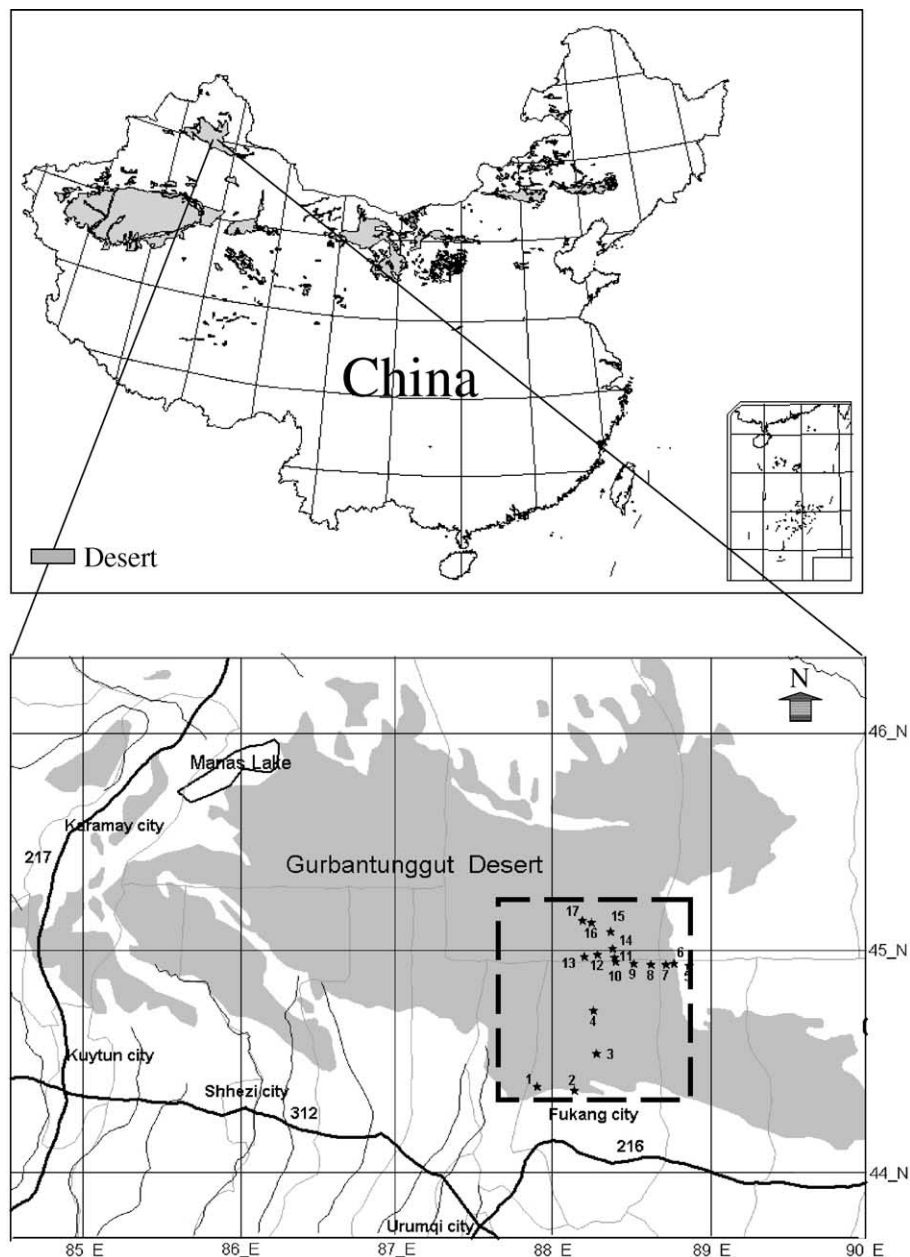


Fig. 1. The study area and sampling locations.

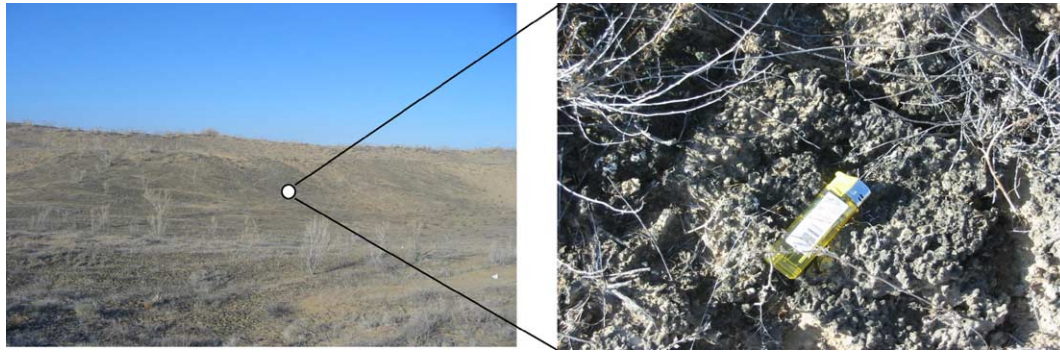


Plate 1. The appearance of the study area and a close-up view of typical biological soil crusts.

focus on the use of remotely sensed data to classify or map biological soil crusts (Green, 1986; Karnieli, 1997; Lewis et al., 2001; Wessels & Van Vuuren, 1986). Although these studies revealed the unique spectral features of biological soil crusts, few studies have made use of their spectral features to develop a robust method for mapping biological soil crusts based on remotely sensed data. One exception is the crust index proposed by Karnieli (1997), who employed remotely sensed data in mapping cyanobacteria dominated biological soil crusts. However, the index is not suitable for lichen-dominated biological soil crusts, which covers large areas in cool and cold deserts (Belnap, 2003), since cyanobacteria are not a dominant species in such crusts.

In this study, the reflectance of lichen-dominated biological soil crusts was measured and used to develop a new index for detecting and mapping the crust distribution. We examined the feasibility of the index for the Landsat ETM+ sensor by using a radiative transfer model (6S) to simulate different coverages of lichen-dominated biological soil crusts under different atmospheric conditions. Then the proposed method was tested with Landsat ETM+ data in the Gurbantonggut Desert, Xinjiang, China.

## 2. Study area and measurement

The Gurbantonggut Desert is situated in the center of the Jungger Basin, Xinjiang Uygur Autonomous Region of China, and is the second largest desert in China, with an area of 48,800 km<sup>2</sup> (Fig. 1). Because of the “Rain shadow” of the Himalayas, moist air currents from the Indian Ocean fail to reach the area, resulting in a vast expanse of arid terrain. Mean annual precipitation is approximately 80 mm, falling predominantly during spring. Mean annual evaporation is 2607 mm. Average temperature is 7 °C. Wind speeds are highest during late spring, averaging 11 m/s, and are predominantly WNW, NW and N. The natural vegetation in the cold desert is shrubland dominated by *Haloxylon ammodendron* and *H. persicum*, etc., with a vegetation cover of less than 30%. The area is covered by huge and dense semi-fixed sand dunes with stable moisture content. There are abundant biological soil crusts on sand surface of the desert, that grow most during wet, cool periods (fall and early spring) when dew, fog or temporary rainfalls, as a moisture source, are available to species relating to the formation of biological soil crusts (Kidron et al., 2002).

Table 1  
Basic condition at the sampling sites

Survey point	Latitude (°)	Longitude (°)	Elevation (m)	Description of sampling point	Fractional cover of sand	Fractional cover of dry vegetation	Fractional cover of biological soil crusts
1	44.3898	87.9018	360	Large area of lichen and moss crusts	25	20	55
2	44.3746	88.1424	447	Large area of lichen crusts	40	15	45
3	44.5416	88.2792	497	Large area of lichen and moss crusts	30	10	60
4	44.7361	88.2638	573	Patch of lichen and moss crusts	50	20	30
5	44.9424	88.8712	504	No crusts	99	1	0
6	44.9478	88.7747	448	sparse algae crusts	90	6	4
7	44.9457	88.7277	530	Patch of lichen and algae crusts	60	5	35
8	44.9446	88.6302	632	Patch of lichen and algae crusts	65	15	20
9	44.9493	88.5179	635	Patch of lichen and algae crusts	75	15	10
10	44.9609	88.4016	679	Patch of lichen and algae crusts	60	10	30
11	44.9764	88.3956	651	Patch of lichen and algae crusts	52	16	32
12	44.9914	88.2901	626	sparse algae crusts	95	2	3
13	44.9801	88.2036	632	Patch of lichen and algae crusts	59	12	29
14	45.0169	88.3863	666	sparse algae crusts	80	10	10
15	45.0961	88.3687	686	Patch of lichen and algae crusts	68	14	18
16	45.1353	88.2513	679	No crusts	98	2	0
17	45.1441	88.1935	657	No crusts	96	4	0

The study was conducted in the southeast of the Gurbantonggut Desert because it contains biological soil crusts typical of that found throughout the desert (Zhang et al., 2002). The appearance of the study area and typical biological soil crusts is shown in Plate 1. Intensive field-work was carried out from 20 to 30 October 2002, during the growth peak of biological soil crusts in the desert. At that time, it was observed that annual plants had died and shrub perennials had dried out. Samples of the most common land surface including biological soil crusts, bare sand, plant litter and dry desert shrubs were collected at 17 sampling sites (Fig. 1). The location and the basic conditions of the sites are given in Table 1. It was observed that most of the sampling sites were up to 60% covered by biological soil crusts, dominated by lichen that covers 90% of the biological soil crusts, and accompanied by moss and algae. Mosses were relatively rare in the northern part of the study area but more common in the southern part. Algae had the opposite distribution pattern. This distribution pattern corresponds with the precipitation pattern, which decreases from south to north. The samples were divided into 5 groups: (1) lichen-dominated biological soil crusts mainly including *Catapyrenium crustosum* (H. Magn.) Wei.comb.nov, *Psora decipiens* (Ehrh.) Hoffm., *Xanthoparmelia desertorum* (Elenkin) Hale (Plate 2b); (2) moss dominated biological soil crusts mainly including *Bryum argenteum* Hedw., *Bryum capillare* Hedw., *Grimmia anodon* B. S. G, *Grimmia pulvinata* (Hedw.) Sm, *Tortula reflexa* Li (Plate 2c); (3) algae dominated biological soil crusts mainly including *Anabaena azotica* Ley, *Chroococcus epiphyticus* Jao, *Lyngbya cryptovaginata* Schk., *Microcoleus vaginatus* (Vauch.) Gom., *Nostoc flagelliforme* Born et Flaf, *Chlorella vulgaris* Beij (Plate 2c); (4) bare sand and (5) dry plant materials. (Here, plant litter and standing dead plants were treated as one category termed “dry plant materials”.) In the dry plant material group, all the typical shrubs (dried but standing) in the area were collected, including *Haloxyylon ammodendron*, *H. persicum*, *Salsola arbuscula*, *Reaumuria soongorica*, *Ephedra distachya*, *Aristida pennata*, *Seriphidium terae-albae*, *Alyssum linifolium*, *Artemisia arenaria*, *Horanowia ulicina*, *Salsola ruthenica*, etc. All the biological soil crusts and bare sand samples were scraped from

the soil surface (3 cm depth) and placed in Petri dishes after visual assessment. Dry plant material samples were cut from standing dead material or gathered from the soil surface. The number of samples in each group was, respectively, 13, 6, 5, 8 and 11. Since there was no rainfall in the period between 1 October and 30 October, almost all the samples were in dry condition.

Spectrum measurements were carried out in situ using an MMS-1 portable spectrometer (Spectra Corp. Co. Ltd., Japan), a double-beam instrument with a cosine-corrected receptor to measure downwelling irradiation simultaneously with the target measurement. To minimize external reflectance or backscatter during measurement, each sample was placed on a black-coated board. The spectrometer was set to provide 2 nm wavelength spectral resolution increments between 400 and 1100 nm and with a 15° field of view (FOV). The spectrometer was held at about 20 cm above the sample, at nadir to ensure each sample covered 100% of the field of view of the sensor. Measurements were taken under clear and sunny condition between 10:00 and 15:00 local time. Measurements were repeated 10 times for each sample while rotating the sample to different angles to counteract roughness and shadowing effects. Measurements were recorded in reflectance mode. Mean reflectance for each sample was calculated as the average of all the replicates for each sample (10 times). In addition to these samples, the spectrum of shadows cast by shrubs was measured in the field survey.

### 3. Methodology

#### 3.1. Spectral features of biological soil crusts, bare sand and dry plant materials

Mean reflectance spectra of the abovementioned 5 group samples as well as the spectra of green plants and shrub shadows are shown in Fig. 2. Generally, all curves except those for green plants and shadows have relatively similar spectral features, but they differ in overall magnitude of reflectance and the depth of the pigment absorption zone. Compared with bare sand and dry plant material, the three

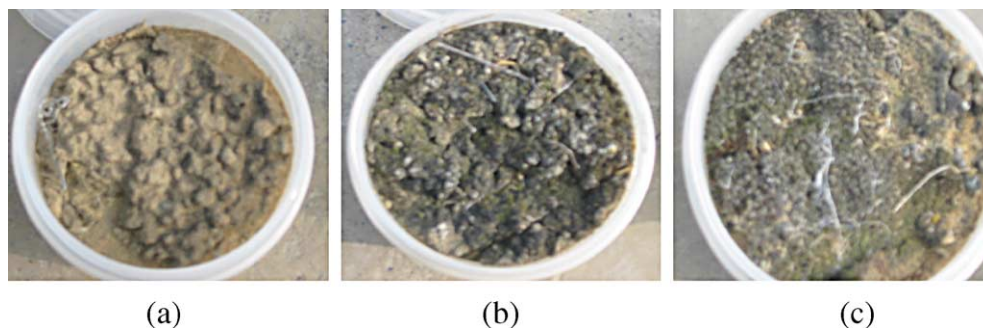


Plate 2. Different biological soil crusts in the study area: (a) a algae-dominated biological soil crusts; (b) a lichen-dominated biological soil crusts; (c) a moss-dominated biological soil crusts.

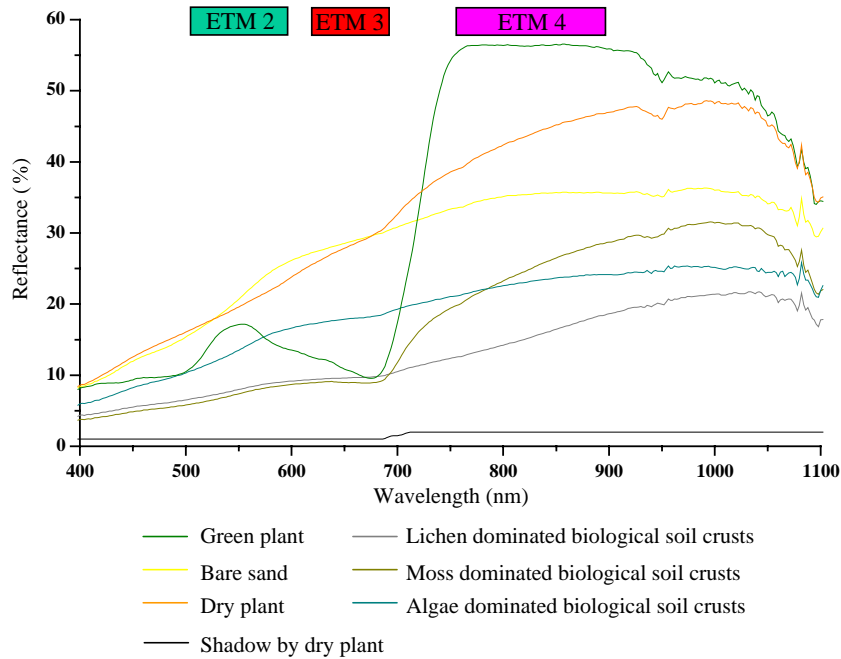


Fig. 2. Reflectance spectra of three biological soil crusts, bare sand, dry plant material and its shadow.

biological soil crusts present a general lower reflectance (below 30%) over the spectrum due to their dark surfaces. Another distinctive feature of the reflectance of three crusts is that they exhibited a slight flattening plateau between 600 and 700 nm, attributable to absorption by photosynthetic pigments. In spite of this characteristic absorption feature of green plants, the biological soil crusts do not show the reflectance peak at 550 nm as is the case with green plants. The phenomenon described by Karnieli (1997) and Karnieli et al. (1999), in which the biological soil crusts has a higher reflectance at blue wavelengths than bare sand does, was not observed in our samples. This may be attributed to the fact that cyanobacteria containing phycobilin pigments do not predominate in the crusts in the study area.

Among the three biological soil crusts, the spectrum of algae dominated biological soil crusts has a higher reflectance than the other two crusts between 400 and 800 nm, also is characterized by a very low absorption at 675 nm. Moss dominated crusts have close to a typical green plant curve but lack a reflectance peak at 550 nm. Dark-colored lichen crusts display the lowest reflectance (below 20%) across the spectrum. All the lichen-dominated biological soil crusts samples exhibited a weak absorption feature at 685 nm. In addition, as observed by Bechtel et al. (2002), as the number of species and the biomass increases, the absorption feature in red wavelengths increases, and overall reflectance (due to crusts darkening) decreases.

In contrast, the spectral behaviors of bare sand and dry plant materials are similar in the VIS-NIR wavebands, relatively low in the blue region (8–15%) and increase gradually towards the near-infrared region (25–40%). The primary difference between bare sand and dry plant material reflectance spectra in the VIS-NIR wavebands is that the

slope of the dry plant material spectrum is slightly steeper than that of bare sand, as observed by Nagler et al. (2000). Unlike green plants, which are dominated by the spectral features of chlorophyll and water, the reflectance of the dry plant materials collected in the study area monotonously climbs from 400 to 1100 nm, attributed to the spectral features of lignin. The spectral features of the dry plant material bear a close resemblance to those of the gray-colored dry plant materials measured by Elvidge (1990), since most of the dry plant material samples were gray-colored. In addition, the spectrum of shadows produced by dry plant materials is uniformly dark with a very low reflectance of about 1% to 2% throughout the wavelengths, almost the same as Leblon et al. (1996) observations.

### 3.2. Development of a new crusts index

Based on observations reported in the previous section, the unique spectral features of the biological soil crusts can be summarized as follows: (1) the slope between the green and red bands of the biological soil crusts is flatter than those of bare sand, dry plant material or green plant; (2) the biological soil crusts have a much lower reflectance at visible and near-infrared bands than those of bare sand, dry plant material or green plant. As a reflection of this knowledge, we developed a biological soil crust index (BSCI) with an aim to exaggerate the difference between biological soil crusts and the background of bare sand, dry plant material or green plant. Specifically, the proposed BSCI is defined as:

$$BSCI = \frac{1 - L \times |R_{red} - R_{green}|}{R_{GRNIR}^{mean}} \quad (1)$$

where  $R_{\text{green}}$ ,  $R_{\text{red}}$  are, respectively, the reflectance of the green and red band, which correspond to bands 2 and 3 for Landsat ETM+ sensor.  $L$  is an adjustment parameter to amplify the absolute difference between  $R_{\text{green}}$  and  $R_{\text{red}}$ . In case the numerator gets a negative value,  $L$  is restricted within the range from 2 to 4. In this study, we assigned 2 as the value of  $L$  based on our observations.  $R_{\text{GRNIR}}^{\text{mean}}$  is the mean reflectance of green, red and the near-infrared band, which subsequently refer to bands 2, 3, 4 for the Landsat ETM+ sensor. In order to remove the effect due to changes in illumination geometry (Huang et al., 2000), all the reflectance items involved in the calculation is the converted surface reflectance, which ranges from 0 to 1.

Specifically, the rationale underneath BSCI is as follows. It can be expected that the value of  $(R_{\text{green}} - R_{\text{red}})$  for biological soil crusts will be much lower than those of bare sand, dry plant material or green plant based on previous observation. After the subtraction from 1, the numerator of the BSCI for biological soil crusts will end up with a relatively larger value as opposed to other types. With regards to the denominator, since biological soil crusts are associated with a uniformly lower reflectance value throughout the visible and near-infrared bands,  $R_{\text{GRNIR}}^{\text{mean}}$  for the soil crusts will stay lower. Compounding the nominator and denominator, the BSCI will present a higher value for biological soil crusts than other types. Based on which the distinction can be made.

In contrast to the Karnieli's Cyanobacteria index (Karnieli, 1997), which was defined as the normalized difference between the RED and the BLUE spectral values:  $CI = 1 - (RED - BLUE) / (RED + BLUE)$ , the BSCI does not include the blue band because in our case lichen-dominated biological soil crusts do not expose a higher reflectance in the blue band (usually as a result of the special phycobilin pigment in cyanobacteria) than the same type of substrate without the biological soil crusts. Given this reason, the BSCI proposed in this study may be particularly useful for the discrimination of the lichen-dominated biological soil crusts from land surface which constitutes of bare sand, dry plant material and green plant.

According to the definition of BSCI and taking into account the spatial resolution of the satellite sensor, it can be expected that the BSCI value would largely depend on the percent coverage of biological soil crusts within a single pixel. As the coverage of the biological soil crusts increases, the value of the index will go up. On the other hand, along with increased coverage of background, the value of the index will keep dropping down until it is indistinguishable from the background. Under certain satellite sensor and atmospheric conditions, there must be a lower-bound detection threshold at which the crusts cannot be distinguished from the background. Similarly, there will also be a saturation threshold (hereafter referred as the upper threshold) at which the coverage of biological soil crusts reach 100%. The upper threshold should be helpful in distinguishing crusted pixels from water pixels or pixels of areas in

shadow generated by clouds and taller dunes, because such pixels have a much higher index value relative to the biological soil crusts, taking into account the much lower reflectance of water and shadow in the green, red and near-infrared bands.

To apply the index to the detection and mapping of biological soil crusts with satellite data, it is necessary to determine the lower and upper thresholds of the index for different sensors and atmospheric conditions. In this study, a rational simulation procedure for Landsat ETM+ sensor was employed for this purpose. Considering the data processing level, the lower and upper thresholds can be determined using different models in two cases: (1) By using surface reflectance data, the case corresponds to using the Landsat ETM+ data after applying full atmospheric correction. (2) By using Top-of-Atmosphere (TOA) reflectance data, the case corresponds to using the Landsat ETM+ data without applying the atmospheric correction due to the lack of accurate measurements of atmospheric optical properties at the time of image acquisition.

### 3.3. Threshold determination using surface reflectance data

Determination of the lower and upper threshold is completed through a simulating of the planetary reflectance of pixel-sized areas of land surface received by a satellite sensor. The simulation was designed based on three assumptions. First, the composite surface reflectance is determined by the summation of reflectance of individual surface components according to their proportional cover relative to the total area of a pixel. Second, there are no atmospheric effects on the radiance received by the satellite sensor. It also means that surface reflectance data are available after applying complete atmospheric correction. Third, there are only four surface components in the study area: biological soil crusts, bare sand, and dry plant material and its shadows. Here, since lichen-dominating biological soil crusts covers 90% of biological soil crusts, the reflectance of lichen-dominating biological soil crusts was used to represent the reflectance of biological soil crusts. Furthermore, although the coverage of dry plant material in the study area is always below 30%, we also took into account the shadow effects produced by dry plant material (mainly shrubs) because the vertical structure of dry plant material has a significant influence on the land surface by shadowing, especially in autumn and winter when sun elevation angle is smaller (Graetz & Gentle, 1982).

According to the following Eq. (2) from the Landsat 7 Science Data Users' Handbook (Irish, 1998), the planetary reflectance ( $\rho_b$ ) received by the ETM+ sensor at band  $b$  can be calculated by normalizing the at-satellite radiance value relative to the irradiance from the sun:

$$\rho_b = \frac{\pi L_b d^2}{ESUN_b \cos(\theta)} \quad (2)$$

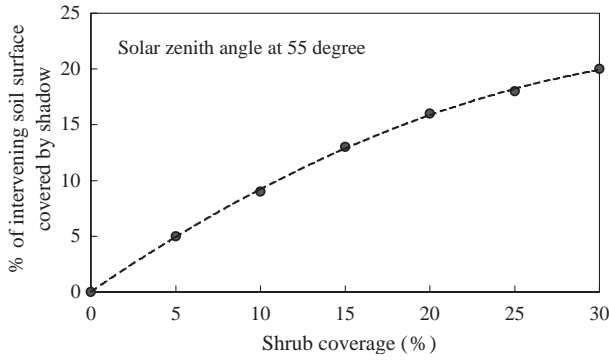


Fig. 3. The relationship between the coverage of shrub and the area of intervening soil surface that is in shadow at a solar elevation angle of 35° (from Graetz & Gentle, 1982).

where  $L_b$  is spectral radiance at sensor band  $b$ ,  $d$  is normalized sun–earth distance on the day of image acquisition,  $\theta$  is the solar zenith angle in degrees, and  $ESUN_b$  is the band-dependent mean solar exo-atmospheric irradiance. The values for  $ESUN_b$  and  $d$  can be taken directly from the Landsat 7 Science Data Users’ Handbook (Irish, 1998). According to the assumption of absence of atmosphere and knowing the Relative Spectral Response function for band  $b$  ( $\lambda_1$  to  $\lambda_2$ ) of the Landsat ETM+ sensor ( $RSR(\lambda)$ ), the radiance ( $L_b$ ) scattered into the upper hemisphere and available for ETM+ sensor can be simply given as:

$$L_b = \frac{\int_{\lambda_1}^{\lambda_2} RSR(\lambda)E(\lambda)\cos(\theta)R(\lambda)d\lambda/\pi d^2}{\int_{\lambda_1}^{\lambda_2} RSR(\lambda)d\lambda} \quad (3)$$

where  $E(\lambda)$  is irradiance at the earth of wavelength  $\lambda$ . It is equal to exo-atmospheric solar irradiance  $E_0(\lambda)$  in a vacuum.  $R(\lambda)$  is surface reflectance. Based on the first assumption, the surface reflectance can be regarded as the composite reflectance ( $R_{com}(\lambda)$ ) of a pixel-sized area of land surface at wavelength  $\lambda$  as:

$$R_{com}(\lambda) = \sum_{i=1}^n p_i \times r_i(\lambda) \quad (4)$$

where  $r_i(\lambda)$  is the reflectance of surface component  $i$  at wavelength  $\lambda$ , and  $p_i$  is the fraction of surface component  $i$  in the pixel. Taking Eqs. (3) and (4) into Eq. (2), the planetary reflectance ( $\rho_b$ ) received by the ETM+ sensor in band  $b$  can be directly simulated from surface composite reflectance as:

$$\rho_b = \frac{\int_{\lambda_1}^{\lambda_2} RSR(\lambda)E_0(\lambda)R_{com}(\lambda)d\lambda}{ESUN_b \times \int_{\lambda_1}^{\lambda_2} RSR(\lambda)d\lambda} \quad (5)$$

Based on Eqs. (1) and (5), several simulations were made to explore the contribution of different coverages of biological soil crusts to planetary reflectance ( $\rho_b$ ) and the BSCI of a pixel-sized area of the land surface. More specifically, the

target pixel was regarded as a mixed pixel formed by biological soil crusts and background including bare sand, dry plant material and its shadows. Here, because we did not investigate the shadowed areas for different vegetation coverage rates during our field survey, a simulation result, originally reported in the study of Graetz and Gentle (1982) was used to obtain the shadowed area for different vegetation coverages assuming a solar zenith angle of 55°, corresponding to autumn (Fig. 3). Based on experience gained in the field survey, we considered four types of background in the study area: (1) bare sand (100%); (2) bare sand (81%), dry plant material (10%) and its shadows (9%); (3) bare sand (64%), dry plant material (20%) and its shadows (16%); (4) bare sand (50%), and dry plant material (30%) and its shadows (20%). Case (4) corresponds to the maximum coverage of dry plant material existing in the study area.

In terms of the simulation results, Fig. 4 shows the BSCI values with different biological soil crusts coverages in four simulation cases. It is evident that the BSCI value increases with biological soil crust coverage in all cases. In addition, as the coverage of dry plant material increases, the shadows generated by dry plant material will have a discernible effect on the BSCI value, causing the BSCI value increase from 3.0 to 3.69 when the biological soil crust coverage equals 0. Therefore, a pixel with a BSCI value of between 3.0 and 3.69 should be regarded as ‘uncertain’ because its BSCI value could be determined either by biological soil crusts or by the shadows cast by dry plant material. Clearly, only pixels with a BSCI value of greater than 3.69 can be reliably identified as crusted pixels, because a shadow itself cannot generate such a large BSCI value. Based on the above simulations and analysis, the lower and upper thresholds of BSCI for using surface reflectance data can be determined as 3.69 and 6.59; and the lowest detection coverage of biological soil crusts is identified as 33%, corresponding to the lower threshold.

#### 3.4. Threshold determination using TOA reflectance data

It is preferable to input the atmospherically corrected surface reflectance for calculating BSCI and determining the

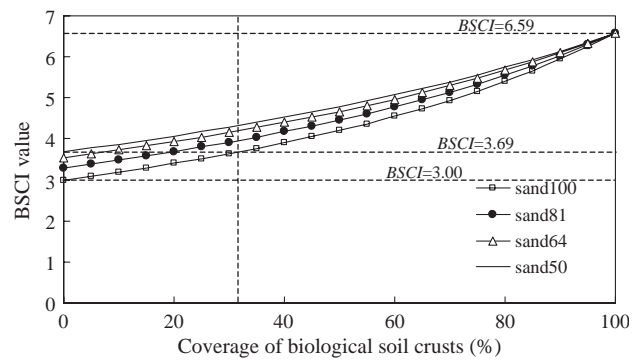


Fig. 4. The relationship between the coverage of biological soil crusts and BSCI value from simulations using surface reflectance data. The simulations were implemented according to four types of background in the study area.

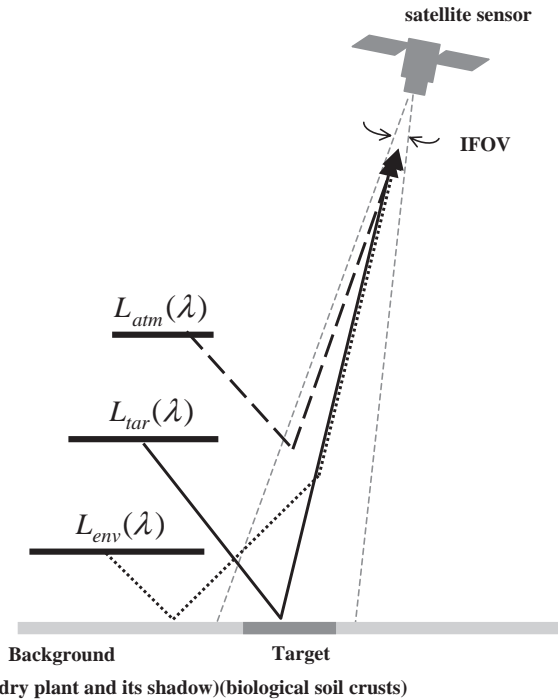


Fig. 5. Components of the radiance received by a satellite sensor for one pixel and the terminology used to identify them in this study.  $L_{tar}$ , the radiance from the biological soil crusts;  $L_{env}$ , the radiance from adjacent pixels; and  $L_{atm}$ , the path radiance (radiance scattered by the atmosphere).

lower and upper threshold. However, atmospheric correction requires accurate measurements of atmospheric optical properties at the time of image acquisition. These measurements are frequently unavailable or of questionable quality, which makes routine atmospheric correction of images difficult with radiative transfer codes, although studies have shown that these radiative transfer codes based on radiative transfer theory can accurately convert satellite measurements to surface reflectance (Ouaidrari & Vermote, 1999). In such application cases, TOA reflectance data have to be used for calculating BSCI and determining the lower and upper threshold. For this reason, we simulated the TOA reflectance of a Landsat ETM+ sensor based on radiative

Table 2  
Parameters used in the simulations based on radiative transfer code (6S)

Sensor condition	
Sensor type	Landsat ETM
Band width	Band 2 (green): 0.52–0.60 ( $\mu\text{m}$ ) Band 3 (red): 0.63–0.69 ( $\mu\text{m}$ ) Band 4 (near IR): 0.76–0.90 ( $\mu\text{m}$ )
Sun zenith angle	55° (fall)
Sun azimuthal angle	158°
Sensor zenith angle	0°
Sensor pass date	Oct. 15
Spatial resolution	30 m
Atmospheric condition	
Atmosphere type	Midlatitude winter
Aerosol type	Continent aerosol model
Aerosol optical depth	0.2 (clear) to 0.8 (hazy)

transfer code 6S (Vermote et al., 1997) under different atmospheric conditions. The simulations were implemented based on assumptions (1) and (3) described in the previous section. Considering photon absorption and scattering in the atmosphere as well as the adjacency effect, the radiance

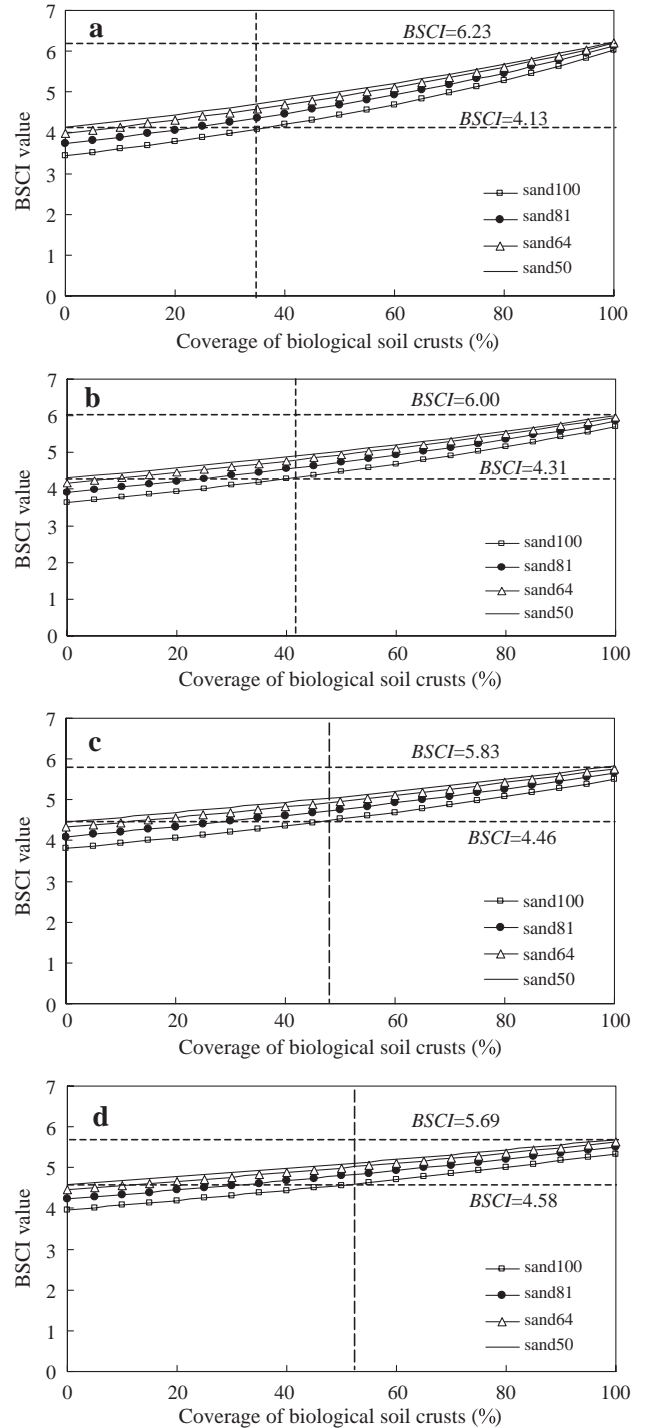


Fig. 6. The relationship between the coverage of biological soil crusts and BSCI value from simulations using TOA reflectance data under different atmospheric conditions. (a) Aerosol optical depth at 550  $\mu\text{m}$  is 0.2 (clear); (2) aerosol optical depth at 550  $\mu\text{m}$  is 0.4; (c) aerosol optical depth at 550  $\mu\text{m}$  is 0.6; (d) aerosol optical depth at 550  $\mu\text{m}$  is 0.8 (hazy).

received by the ETM+ sensor was divided into the three components shown in Fig. 5. By using the 6S code, in which the Relative Spectral Response function of the Landsat ETM+ sensor was used instead of that of the TM sensor, the three components of radiance can be calculated, after which the planetary reflectance ( $\rho_b$ ) received by the ETM+ sensor can be calculated by normalizing at-satellite radiance values relative to irradiance from the sun. Table 2 shows the parameters for simulations corresponding to autumn conditions in the Gurbantonggut Desert.

The simulation results are shown in Fig. 6. The relationship can be seen between BSCI values and biological soil crusts coverage under different atmospheric conditions, in which aerosol optical depth at 550  $\mu\text{m}$  varies from 0.2 (clear) to 0.8 (hazy). As in Fig. 6, the BSCI value increases with increasing biological soil crust coverage under all atmospheric conditions. However, the range of BSCI corresponding to biological soil crusts coverage from 0% to 100% becomes smaller and smaller with increasing aerosol optical depth. This can be attributed to the fact that the interference caused by absorption and scattering in the atmosphere as well as the adjacency effect reduces the contribution coming directly from the target pixel to TOA reflectance. In short, poor atmospheric conditions diminish the sensitivity of the BSCI index with respect to biological soil crust detection. As described in the previous section, the lower and upper thresholds of BSCI for using TOA reflectance data can be determined as 4.13 and 6.23 for an aerosol optical depth of 0.2; 4.32 and 6.00 for an aerosol optical depth of 0.4; 4.46 and 5.83 for an aerosol optical depth of 0.6; and 4.58 and 5.69 for an aerosol optical depth of 0.8. Similarly, the lowest detection coverage of biological soil crusts can be identified as 37%, 42%, 47% and 52%, respectively, corresponding to the lower thresholds for different atmospheric conditions. A comparison of the results in Figs. 4 and 6 clearly shows that calculation of

BSCI using surface reflectance data after atmospheric correction provides a better biological soil crust detection than that using TOA reflectance data without atmospheric correction.

#### 4. Mapping lichen-predominating biological soil crusts in the Gurbantonggut Desert using Landsat ETM+ data

##### 4.1. Data and processing

To validate the applicability of BSCI index to biological soil crusts mapping, one scene of Landsat 7 ETM+ image data (path/row: 142/29, 18 October 2002) covering the whole study area with good image quality was acquired and used. Auxiliary data were also collected, including 1:50,000 topographic maps and GPS survey data from October 2002 and April 2003. The ETM+ image was geometrically corrected to the UTM projection, which has 30 $\times$ 30 m resolution, the study area was clipped from the image using the boundary of the study area digitized into a GIS database.

After that, the raw digital numbers (DN) of the Landsat ETM+ image were converted to physical meaningful reflectance values according the Landsat 7 Science Data Users' Handbook (Irish, 1998). First, digital numbers were converted to at-satellite radiance. Second, the at-satellite radiance values were normalized relative to irradiance from the sun, which results in (unitless) TOA reflectance values.

An operational atmospheric correction for Landsat TM data proposed by Ouaidrari and Vermote (1999) was employed to convert the TOA reflectance to surface reflectance. This correction method is based on the 6S radiative transfer code and can make corrections for atmospheric and adjacency effects. The 6S radiative transfer code was run with a mid-latitude winter standard atmosphere and continental aerosol model. The aerosol optical

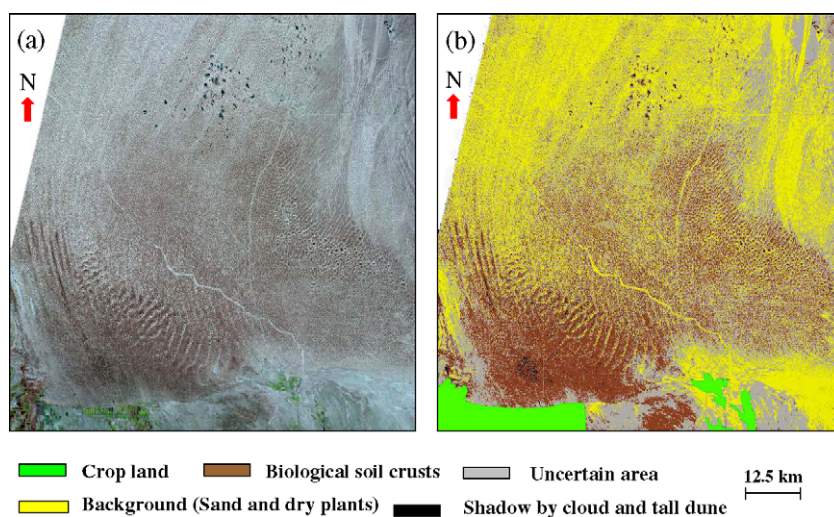


Fig. 7. The distribution of biological soil crusts in the study area detected by BSCI. (a) RGB composition image of study area (TM bands 5, 4, and 3 in 2002). (b) Classification of biological soil crusts in the study area.

depth (AOD) was extracted from the ETM+ image itself, using the dense dark vegetation (DDV) approach (Kaufman & Sendra, 1988).

After obtaining the surface reflectance, the BSCI was calculated for each pixel of Landsat ETM+ image, respectively. The lower and upper thresholds of BSCI for using surface reflectance data were then used to extract the area of more than 33% covered by biological soil crusts. Furthermore, pixels with BSCI values between 3.0 and 3.69 were identified as uncertain areas that also may have been less than 33% covered by biological soil crusts. The pixels with BSCI values that exceed 6.59 were identified as cloud and tall dune shadow areas. Because biological soil crusts do not exist in agricultural land, croplands were excluded by visual interpretation. The finally classified result is shown in Fig. 7.

#### 4.2. Result analysis and accuracy assessment

As indicated by Fig. 7, the distribution of biological soil crusts in the study area can be found out in two aspects: (1) biological soil crusts are mainly distributed in the southwest region of the study area, and exhibit a decreasing trend from the southwest to the north and east. The biological soil crusts almost disappear in the north of the study area. (2) Biological soil crusts are continuously distributed in the southwest of the study area but its distribution pattern becomes patchier in the northern and eastern part. The distribution characteristics of biological soil crusts from Landsat ETM+ images are almost identical to our field survey observations. At this point, the reason why biological soil crusts display such distribution characteristics is still unknown, and needs to be explored in the future. We also found several errors in our classification, notably at the edges of cloud shadows and dune shadows, where shadows were erroneously identified as biological soil crusts.

To evaluate the performance of the proposed BSCI, the accuracy of the classification was estimated at ‘crusted/uncrusted’ levels using the field survey data. Table 3 shows an error matrix of ‘crusted/uncrusted’ detection constructed of 76 GPS points obtained in the field survey carried out in October 2002 and April 2003. A Kappa coefficient of 0.82 and an overall accuracy of 94.7% were achieved. Although the number of GPS points was only 76, the high Kappa coefficient and overall accuracy suggest that the new index

effectively identifies lichen-dominating biological soil crusts, and therefore has major potential for use in other cool and cold deserts for biological soil crusts detection and mapping.

## 5. Conclusion

A biological soil crusts covering the soil surface has been observed widely in desert areas all over the world. Despite its unassuming appearance, the biological soil crusts are critical to support many processes in the past and present desert ecosystems. Due to its ecological importance and vulnerability to disturbance, mapping the distribution of biological soil crusts becomes an increasingly demanded task to support its protection in the desert regions. In this study, based on our field survey measurements, we developed a new index (BSCI) for detecting and mapping the crust distribution, employing its unique spectral features. The index can be treated as an enhancement of spectral features of the biological soil crusts in green, red and near infrared. It yields higher values for the biological soil crusts relative to the background of bare sand and dry plant material. Through the simulations of planetary reflectance received by the ETM+ sensor under different atmospheric conditions, it is concluded that the new index is applicable to detection and mapping of crust distribution; however, under poor atmospheric conditions, the sensitivity of the BSCI index will decrease, and the lowest detection coverage of biological soil crusts will increase. It is recommended to calculate BSCI and determine the lower and upper threshold using surface reflectance after atmospheric correction.

Although the new index also exhibits a lower value for green plants due to their higher reflectance in the green and near-infrared bands, taking into account the fact that the biological soil crusts is possibly in a dormant condition when plants are in their growth season, we recommend use of the index in the growth period of the biological soil crusts (fall and early spring). Furthermore, it is worth noting that the index can only be applied to desert areas because mixed pixels for green plants, water or wetlands in other areas can exhibit higher BSCI values and risk being confused with biological soil crusts. In addition, when the new index is applied to other satellite sensors or other cool and cold deserts with different land surface components, the lower and upper detection thresholds should be determined empirically using individual simulations.

Although a Kappa coefficient of 0.82 and an overall accuracy of 94.7% for ‘crusted/uncrusted’ detection were achieved in our case study in the Gurbantonggut Desert, Xinjiang, China, it cannot be predicted that all lichen-dominating biological soil crusts will be distinguishable using this approach. A much larger sample of lichen-dominating biological soil crusts from various study sites also needs be measured and compared using the new index. This would provide more accurate separation of lichen-dominating biological soil crusts from the background.

Table 3

Error matrix for ‘crusted/uncrusted’ detection by 76 GPS points obtained in the field survey

Reference data					
		No crusted points	Crusted points	Sum	Commission error
Detected results	No crusted points	11	4	15	26.67
	Crusted points	0	61	61	0.00
	Sum	11	65	76	
	Omission error	0.00	6.15		

Overall accuracy=94.74%; Kappa coefficient=0.82.

## Acknowledgments

This research was partially supported by National Nature Science Foundation of China (No. 90202019) and the Young Scientist Program of the National Institute for Environmental Studies, Japan.

## References

- Ager, C. M., & Milton, N. M. (1987). Spectral reflectance of lichens and their effects on the reflectance of rock substrates. *Geophysics*, *52*, 898–906.
- Bechtel, R., Rivard, B., & Sanchez-Azofeifa, A. (2002). Spectral properties of foliose and crustose lichens based on laboratory experiments. *Remote Sensing of Environment*, *82*(2–3), 389–396.
- Belnap, J. (2003). The world at your feet: Desert biological soil crusts. *Frontiers in Ecology and the Environment*, *1*(5), 181–189.
- Belnap, J., & Eldridge, D. (2001). Disturbance and recovery of biological soil crusts. In J. Belnap, & O. L. Lange (Eds.), *Biological soil crusts: Structure, function, and management* (pp. 363–383). Berlin: Springer-Verlag.
- Belnap, J., Kaltenecker, J. H., Rosentreter, R., Williams, J., Leonard, S., Eldridge, D. (2001). Biological soil crusts: ecology and management. Technical Reference 1730-2, U.S. Department of the Interior.
- Brotherson, J. D., Rushforth, S. R., & Johansen, J. R. (1983). Effects of long-term grazing on cryptogam crust cover in Navajo National Monument, Ariz. *Journal of Range Management*, *36*, 579–581.
- Eldridge, D. J., & Greene, R. S. B. (1994). Microbiotic soil crusts: A review of their roles in soil and ecological processes in the rangelands of Australia. *Australian Journal of Soil Research*, *32*, 389–415.
- Elvidge, C. D. (1990). Visible and near-infrared reflectance characteristics of dry plant materials. *International Journal of Remote Sensing*, *11*, 1775–1795.
- Friedmann, E. I., & Galun, M. (1974). Desert algae, lichens and fungi. G. W. Brown (Ed.), *Desert biology II* (pp. 165–212). New York: Academic Press.
- Graetz, R. D., & Gentle, M. R. (1982). The relationship between reflectance in the Landsat wavebands and the composition of an Australian semi-arid shrub rangeland. *Photogrammetric Engineering and Remote Sensing*, *48*, 1721–1730.
- Green, G. M. (1986). Use of SIR-A and Landsat MSS data in mapping shrub and intershrub vegetation at Koonamore, South Australia. *Photogrammetric Engineering and Remote Sensing*, *52*, 659–670.
- Huang, C., Wylie, B., Yang, L., Homer, C., & Zylstra, G. (2000). Derivation of a tasseled cap transformation based on Landsat 7 at-satellite reflectance. USGS EROS Data Centre, Internet source: <http://landcover.usgs.gov/pdf/tasseled.pdf>
- Irish, R. (1998). Landsat 7 Science Data Users Handbook. Internet source: [http://ftpwww.gsfc.nasa.gov/IAS/handbook/handbook\\_toc.html](http://ftpwww.gsfc.nasa.gov/IAS/handbook/handbook_toc.html)
- Jacobberger, P. A. (1989). Reflectance characteristics and surface processes in stabilized dune environments. *Remote Sensing of Environment*, *28*, 287–295.
- Johansen, J. R. (1993). Minireview: Cryptogamic crusts of semiarid and arid lands of North America. *Journal of Phycology*, *29*, 139–147.
- Johansen, J. R., Ashley, J., & Rayburn, W. R. (1993). The effects of range fire on soil algal crusts in semiarid shrub-steppe of the Lower Columbia Basin and their subsequent recovery. *Great Basin Naturalist*, *53*, 73–88.
- Karnieli, A. (1997). Development and implementation of spectral crust index over dune sands. *International Journal of Remote Sensing*, *18*, 1207–1220.
- Karnieli, A., Kidron, G. J., Glaesser, C., & Ben-Dor, E. (1997). Spectral characteristics of cyanobacterial soil crust in the visible, near infrared and short wave infrared (400–2500 nm) in semiarid environments. *Twelfth International Conference and Workshops on Applied Geologic Remote Sensing, vol. II* (pp. 417–424). Denver, Colorado.
- Karnieli, A., Kidron, G. J., Glaesser, C., & Ben-Dor, E. (1999). Spectral characteristics of cyanobacteria soil crust in semiarid environments. *Remote Sensing of Environment*, *69*, 67–75.
- Karnieli, A., Kokaly, R., West, N. E., & Clark, R. N. (2001). Remote sensing of biological soil crusts. J. Belnap, & O. L. Lange (Eds.), *Biological soil crusts: Structure, function, and management* (pp. 431–455). Berlin: Springer-Verlag.
- Karnieli, A., Shachak, M., Tsoar, H., Zaady, E., Kaufman, Y., Danin, A., & Porter, W. (1996). The effect of microphytes on the spectral reflectance of vegetation in semiarid regions. *Remote Sensing of Environment*, *57*, 88–96.
- Karnieli, A., & Tsoar, H. (1995). Satellite spectral reflectance of biogenic crust developed on desert dune sand along the Israel–Egypt border. *International Journal of Remote Sensing*, *16*, 369–374.
- Karnieli, K., & Sarafis, V. (1996). Reflectance spectrometry of cyanobacteria within soil crusts—a diagnostic tool. *International Journal of Remote Sensing*, *8*, 1609–1615.
- Kaufman, Y. J., & Sendra, C. (1988). Algorithm for automatic atmospheric correction to visible and near-IR satellite imagery. *International Journal of Remote Sensing*, *9*, 1357–1381.
- Kidron, G. J., Herrnstadt, I., & Barzilay, E. (2002). The role of dew as a moisture source for sand microbiotic crusts in the Negev Desert, Israel. *Journal of Arid Environment*, *52*, 517–533.
- Leblon, B., Gallant, L., & Granberg, H. (1996). Effects of shadowing types on ground-measured visible and near-infrared shadow reflectances. *Remote Sensing of Environment*, *58*, 322–328.
- Lewis, M., Jooste, V., & de Gasparis, A. A. (2001). Discrimination of arid vegetation with airborne multispectral scanner hyperspectral imagery. *IEEE Transactions on Geoscience and Remote Sensing*, *39*, 1471–1479.
- Nagler, P. L., Daughtry, C. S. T., & Goward, S. N. (2000). Plant litter and soil reflectance. *Remote Sensing of Environment*, *71*, 207–215.
- O’Neill, A. L. (1994). Reflectance spectra of microphytic soil crusts in semiarid Australia. *International Journal of Remote Sensing*, *15*, 675–681.
- Ouaidrari, H., & Vermote, E. F. (1999). Operational atmospheric correction of Landsat TM data. *Remote Sensing of Environment*, *70*, 4–15.
- Pinker, R. T., & Karnieli, A. (1995). Characteristic spectral reflectance of a semi-arid environment. *International Journal of Remote Sensing*, *16*, 1341–1363.
- Rollin, E. M., Milton, E. J., & Roche, P. (1994). The influence of weathering and lichen cover on the reflectance spectra of granitic rocks. *Remote Sensing of Environment*, *50*, 194–199.
- Tsoar, H., & Karnieli, A. (1996). What determines the spectral reflectance of the Negev-Sinai sand dunes. *International Journal of Remote Sensing*, *17*, 513–525.
- Vermote, E. F., Tanré, D., Deuzé, J. L., Herman, M., & Morcrette, J.-J. (1997). Second simulation of the satellite signal in the solar spectrum, 6S: An overview. *IEEE Transaction of Geoscience and Remote Sensing*, *35*, 675–686.
- Wessels, D. C. J., & Van Vuuren, D. R. J. (1986). Landsat imagery—its possible use in mapping the distribution of major lichen communities in the Namib Desert, South West Africa. *Madoqua*, *14*, 369–373.
- West, N. E. (1990). Structure and function of microphytic soil crusts in wildland ecosystems of arid to semi-arid regions. *Advances in Ecological Research*, *20*, 179–223.
- Zhang, Y. M., Cao, T., & Pan, B. R. (2002). A study on bryophyte associated with formation of soil crust in south fringe of Gurbantunggut Desert in Xinjiang, China. *Acta Botanica Boreali-Occidentalia Sinica*, *22*, 18–23.